Velocity distribution and hydrodynamic drag in turbulent flow

Evgenii Ignatenko[1], *Yuliya* Bryanskaya[1*], and *Ilya* Bryansky[2]

[1]National research Moscow State University of Civil Engineering, Hydraulics and Hydraulic Engineering department, 129337 Yaroslavskoe highway 26, Russia
[2]Design company Giprorechtrans Ltd., 20 Bobur st., Uzbekistan

Abstract. This work aims to study the vertical velocity distribution in the near-wall layer of a pipe, channel, and boundary layer of a flat plate because these issues are of great practical and theoretical importance. Until now, engineering calculations of turbulent flows have been based on empirical formulas derived in the last century. The theory of turbulent fluid motion has not been completed, and the issues of velocity distribution and hydraulic resistance remain open for further study. It is known that velocity distribution in the flow is intricately linked to hydraulic resistance. Therefore, the study's objectives also include determining the position of the point of maximum turbulent tangential stresses and comparing the change in tangential stresses with the logarithmic velocity profile. Based on calculation and analytical methods, we have researched the distribution of the turbulent component of the tangential stress along the depth of the flow. Derived an expression determining the position of the maximum point of the turbulent component of the tangential stress for smooth tubes. The contribution of the viscous component of the tangential stress at different points along the flow depth has been evaluated. The calculation results determining the position of the maximum point of the turbulent component of the tangential stress were compared with experimental data on velocity distribution in the flow. With the decrease of the hydraulic resistance coefficient, the point of maximum turbulent tangential stresses shifts towards the solid flow boundary. Based on the results of comparing the maximum turbulent tangential stresses with the total tangential stress, we can conclude that the contribution of the viscous component of the tangential stress to the total amount of friction and its influence on velocity distribution is significant. The angular coefficient of the velocity profile for the flow core is determined.

1 Introduction

Knowing the patterns of velocity distribution for a cross-section of a stream is crucial for solving a number of theoretical and practical problems of hydrometry and hydraulic engineering. The pattern of average velocity distribution for vertical lines in the flow field has a significant practical value. The time-averaged velocity in vertical lines is linked with

* Corresponding author: mgsu-hydraulic@yandex.ru

problems of determining the discharge and flow circulation strength on the curve, calculating riverbed erosion and carrying capacity of the stream, as well as other important matters [1,2].

The matters connected with velocity distribution and hydrodynamic drag for the moving fluid are considered well-studied [3-16]. However, to date, the engineering calculations are based on half-empiric turbulent theories that were made in the first half of the 20th century. One of the most famous and highly-demanded theories is Prandtl's turbulence theory. Nowadays, results of experimental research allow us to divide turbulent flow into the following sections: a viscous sublayer adjacent to the boundary surface, a near-wall region adjacent to the viscous sublayer, and a peripheral area of the flow that lies above the near-wall region [17].

It is also worth noting that velocity distribution and hydrodynamic drag formulas are interdependent and should not contradict each other.

2 Materials and methods

It is known for a fact that velocity distribution in the near-wall region in the vicinity of the solid flow boundary is compliant with the logarithmic law that results from Prandtl's half-empiric theory:

$$u = \frac{u_*}{\kappa} \ln y + C , \qquad (1)$$

where $u_* = \sqrt{\frac{\tau_0}{\rho}}$ is dynamic velocity, τ_0 is skin friction drag of the solid flow boundary, and κ is Karman parameter.

The half-empiric theory was based on several conformable apriori postulates. Therefore the accuracy and versatility of logarithmic velocity distribution were questioned by various researchers that proposed different corrections [18, 19] for the velocity profile (1). Nowadays, the velocity profile (1) is considered applicable not for the whole flow but only for the near-wall layer l_p, the width of which is roughly 15% of the pipe radius r_0, or of the flow depth in the channel h, or of the width of the boundary layer δ, that appears while flowing around a flat plate. However, there were yet no attempts to computationally and analytically ground the width of the said l_p layer, which due to understandable circumstances, can be named the Prandtl layer.

At the same time, the flow in the near-wall Prandtl layer has several physical features that allow us to suggest a computing model determine l_p. One of the notable peculiarities of this layer is the non-stationarity flow in the viscous sublayer that constitutes a rather small part of the near-wall layer and which occurs mostly in viscous friction [14]. Later researches [20] showed that the flow in the viscous sublayer is interlacing, with an alternation of viscous (laminar) and turbulent flow states. When the viscous sublayer becomes turbulent, the momentum transfer mechanism from the flow to the solid boundary changes. The further from the solid boundary, the longer and more intense the flow turbulence. At the same time, the number of turbulent components in total skin friction drag balance grows while its viscous component drops [21]. Further from the solid boundary, the total skin friction drag is primarily determined by the turbulent component of the flow drops. This means that turbulent skin friction drag reaches its maximum at some distance from the solid flow boundary (Fig. 1).

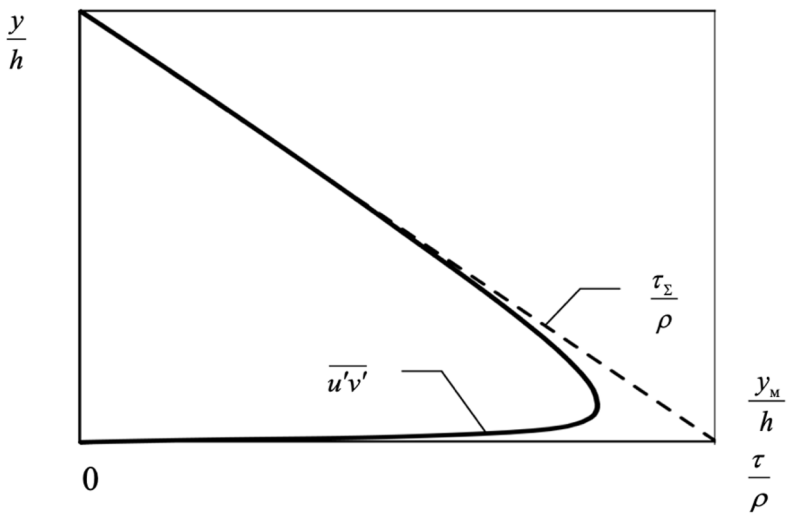

Fig. 1. Skin friction drag balance.

3 Results

Considering the linear scaling of total skin friction drag along the pipe radius r_0, the formula can be written as

$$u_{*0}^2\left(1-\frac{y}{r_0}\right)=\nu_B\frac{du}{dy}+\nu_T\frac{du}{dy}, \qquad (2)$$

where ν_B is kinematic viscosity and ν_T is turbulent viscosity.

This equation for total skin friction drag is derived from Newton-Boussinesq's idea and is open for critique. Newton proposed that there is a causal relationship between skin friction drag and velocity gradient that occurs in the flow. In this case, velocity gradient is mostly created by turbulent skin friction drag, and formula (2) connects it with skin friction drag of viscous nature to the same degree. This mistaken assumption is used in many hydraulics course books.

The velocity gradient that is normal against the wall $\frac{du}{dy}$ can be found as a derivation from the equation (1):

$$\frac{du}{dy}=\frac{u_*}{\kappa}\frac{1}{y}. \qquad (3)$$

Then the turbulent component of skin friction drag τ_T can be found as the difference between total skin friction drag and its viscous component

$$\frac{\tau_T}{\rho}=u_*^2\left(1-\frac{y}{r}\right)-\nu_B\frac{u_*}{\kappa}\frac{1}{y}. \qquad (4)$$

Taking the derivative from the equation (4) with the first order derivative equal to zero

$$\frac{d}{dy}\left(\frac{\tau_T}{\rho}\right) = -\frac{u_*^2}{r} + \nu_B \frac{u_*}{\kappa}\frac{1}{y_M^2} = 0, \tag{5}$$

we can determine the coordinates of the maximum turbulent skin friction point

$$\kappa\left(\frac{y_M}{r_0}\right)^2 \frac{u_{*0} r_0}{\nu_B} = 1. \tag{6}$$

Then by taking the logarithm of this expression with κ_1=0.4 we get

$$2\ln\frac{y_M}{r_0} = \ln 2{,}5 - \ln\frac{u_* r_0}{\nu_B}. \tag{7}$$

For further analysis, we consider the flow in smooth pipes using the famous formula for smooth pipe drag

$$\frac{1}{\sqrt{\lambda}} = 2\lg \mathrm{Re}\sqrt{\lambda} - 0{,}8, \tag{8}$$

where $\mathrm{Re}\sqrt{\lambda}$ can be expressed as

$$\mathrm{Re}\sqrt{\lambda} = \frac{V \cdot 2r_0}{\nu_B}\frac{\sqrt{\lambda}\sqrt{8}}{\sqrt{8}} = \frac{u_{*0} r_0}{\nu}\cdot 2\sqrt{8}. \tag{9}$$

Taking into account the correlation between (8) and (9), we get

$$\ln\frac{u_{*0} r_0}{\nu_B} = \frac{1{,}15}{\sqrt{\lambda}} - 0.82, \tag{10}$$

$$\frac{1}{\sqrt{\lambda}} = 0.71 + \ln\frac{u_* r_0}{\nu}. \tag{11}$$

If we place the expression (11) in equation (9), we find

$$\ln\frac{y_M}{r_0} = \frac{1}{2}\ln 2.5 - \frac{0.575}{\sqrt{\lambda}} + 0.41, \tag{12}$$

or the final form of the formula

$$\ln\frac{y_M}{r_0} = 0.87 - \frac{0.575}{\sqrt{\lambda}}. \tag{13}$$

Calculation results from the acquired formula (13) are shown in Fig. 2. According to them, with the average coefficient values λ=0.03÷0.05 that often occur in practice, the

maximum of turbulent skin friction drag is located at the distance of y_M=(0.1÷0.15)r_0, which concords with the data from the suggested corrections [18, 19] for the logarithmic velocity profile for $\frac{y}{r_0} > 0{,}15$ mentioned above.

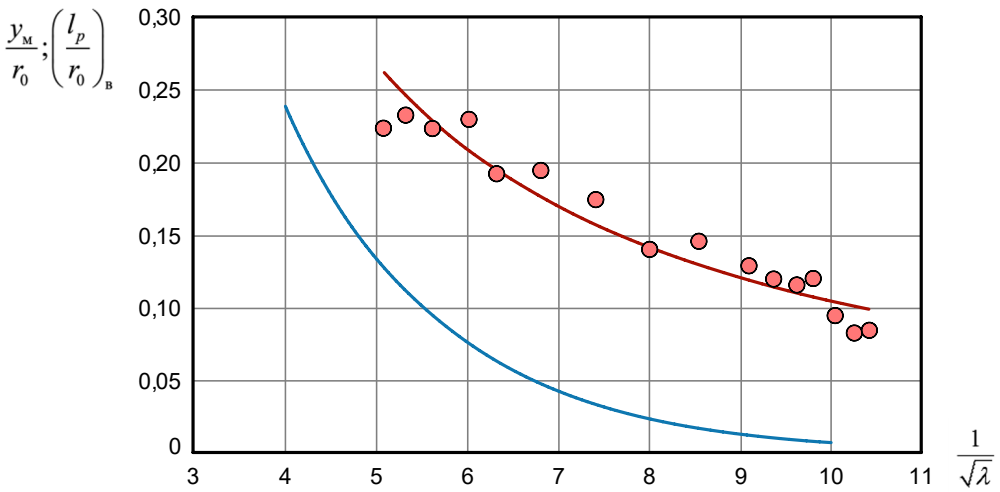

Fig. 2. Calculation results from the acquired formula (13)

It is worth noting, however, that the λ is lower, the closer to the solid flow boundary shifts the position of the maximum turbulent skin friction drag point.

Considering equations (3) and (5), we can determine the contribution of the turbulent component to the total amount of skin friction drag. The relationship (3) can be expressed as

$$\frac{\tau_T}{\rho} = u_{*0}^2 \left[1 - \frac{y}{r_0} - \frac{1}{\kappa} \frac{\nu_B}{u_* y}\right], \tag{14}$$

and using formula (5)

$$\frac{1}{\kappa} \frac{\nu_B}{u_* y_M} = \frac{y_M}{r_0}, \tag{15}$$

we get the following correlation in the point of maximum turbulent skin friction drag

$$\frac{\tau_{T\max}}{\rho u_{*0}^2} = \left[1 - 2\frac{y_M}{r_0}\right], \tag{16}$$

The calculation results for the correlation (16) for various $\frac{y_M}{r_0}$ taken considering the estimates above are shown in Table 1.

Table 1. The calculation results for the correlation (16) for various $\frac{y_M}{r_0}$

$\frac{y_M}{r_0}$	0.5	0.1	0.15	0.2	0.25
$\frac{\tau_{T\max}}{\rho u_{*0}^2}$	0.9	0.8	0.7	0.6	0.5

The total amount of skin friction drag changes depending on the distance from the wall. Therefore, it would be more accurate to compare $\tau_{T\max}$ with total skin friction drag τ_Σ where $y=y_M$ that equals $\rho u_{*0}^2\left(1-\frac{y_M}{r_0}\right)$. The results of this comparison are shown in Table 2.

Table 2. Comparison $\tau_{T\max}$ with total skin friction drag τ_Σ

$\frac{y_M}{r_0}$	0.05	0.1	0.15	0.2	0.25
$\frac{\tau_{T\max}}{\rho u_{*0}^2\left(1-\frac{y_M}{r_0}\right)}$	0.947	0.89	0.82	0.75	0.67

The data shows that the contribution of viscous components to the total amount of skin friction drag and its impact on velocity distribution at the point of maximum turbulent skin friction drag is quite significant.

Using the expressions above, we can evaluate the contribution of turbulent components to the total amount of skin friction drag τ_Σ in other points of the flow.

The equation (7) can be expressed as

$$\frac{\tau_T}{\rho}=\frac{\tau_\Sigma}{\rho}-\frac{1}{\kappa}\frac{u_{*0}\nu_B}{y}, \tag{17}$$

where $\frac{\tau_\Sigma}{\rho}=u_{*0}^2\left(1-\frac{y}{r_0}\right)$ we can find

$$\frac{\tau_T}{\tau_\Sigma}=1-\frac{1}{\kappa}\frac{u_{*0}\nu_B}{y\frac{1}{\rho}\tau_\Sigma}=1-\frac{1}{\kappa}\frac{1}{\frac{u_{*0}r_0}{\nu_B}\frac{y}{r_0}\left(1-\frac{y}{r_0}\right)} \tag{18}$$

Using the connection between $\frac{u_{*0}r_0}{\nu_B}$ and drag coefficient λ expressed as (10), we can calculate $\frac{\tau_T}{\tau_\Sigma}$ for various λ values with κ=0.4. The results are presented in Table 3.

Table 3. Results of calculations $\frac{\tau_T}{\tau_\Sigma}$ for various λ values

$\frac{y}{r_0}$	0.01	0.05	0.1	0.15	0.2	0.25	0.3	0.4	0.5	0.6
λ=0.01 $\frac{u_{*0}r_0}{\nu_B}$ =43478	0.994	0.999								
λ=0.015 $\frac{u_{*0}r_0}{\nu_B}$ =4402	0.943	0.988	0.994	0.996						
λ=0.02 $\frac{u_{*0}r_0}{\nu_B}$ =1498	0.831	0.96	0.981	0.987	0.99					
λ=0.03 $\frac{u_{*0}r_0}{\nu_B}$ =337		0.84	0.918	0.942	0.954	0.96	0.965	0.969		
λ=0.04 $\frac{u_{*0}r_0}{\nu_B}$ =138.4		0.62	0.80	0.86	0.89	0.9	0.914	0.925	0.928	0.925

The calculated data in Table 3 show that with $\frac{y}{r_0} > 0.05$ when λ<0.02, the percent of turbulent component is more than 95–99% of the total amount of skin friction drag. With the increase of λ value, the contribution of viscous component grows and exceeds 4–5% till $\frac{y}{r_0} \sim 0.25 \div 0.30$.

It is also interesting to compare the experimental value of Prandtl's layer width calculated via velocity profiles measured by Nikuradse in smooth pipes with the calculated results acquired from measuring turbulent and viscous components of skin friction drag. Experimental values of $\left(\frac{l_p}{r_0}\right)_B$ were calculated based on either the location of deviation of Prandtl-Nikuradse's logarithmic experimental points or the points where the near-wall flow area crossed the logarithmic approximation of flow core velocity distribution (Fig. 3). The $\left(\frac{l_p}{r_0}\right)_B$ values that were calculated using this method are shown in table 4 and Fig. 2.

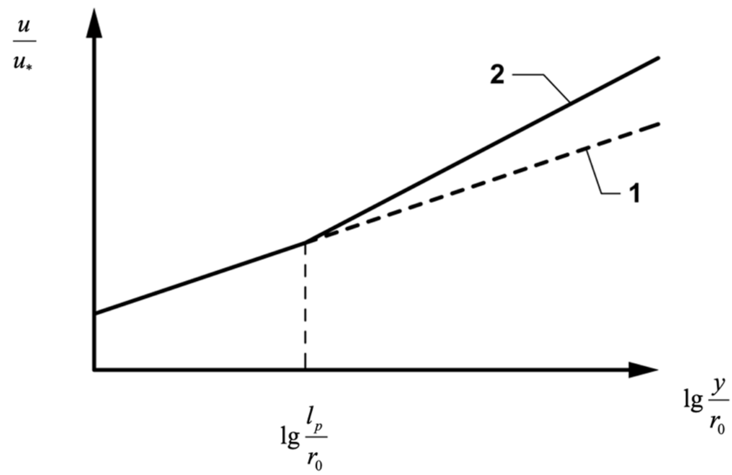

Fig. 3. Determination of experimental values $\left(\frac{l_p}{r_0}\right)_B$

1 is Nikuradse's logarithmic profile; *2* is deviation from the real velocity profile.

Table 4. Results of calculations $\left(\frac{l_p}{r_0}\right)_B$

d, cm	$Re \cdot 10^3$	$\lambda \cdot 10^2$	$\nu \cdot 10^2$, cm²/sec	u_{*0}, cm/sec	$\frac{u_{*0} r_0}{\nu_B}$	$\left(\frac{l_p}{r_0}\right)_B$	$\left(\frac{\tau_T}{\tau_\Sigma}\right)_p$
1	4.0	3.88	1	4.0	3.88	1	4.0
1	6.1	3.53	1	6.1	3.53	1	6.1
1	9.2	3.17	1	9.2	3.17	1	9.2
1	4.0	3.88	1	4.0	3.88	1	4.0
1	6.1	3.53	1	6.1	3.53	1	6.1
1	9,2	3.17	1	9.2	3.17	1	9.2
1	4.0	3.88	1	4.0	3.88	1	4.0
1	6.1	3.53	1	6.1	3.53	1	6.1
1	9.2	3.17	1	9.2	3.17	1	9.2
1	4.0	3.88	1	4.0	3.88	1	4.0
1	6.1	3.53	1	6.1	3.53	1	6.1
1	9.2	3.17	1	9.2	3.17	1	9.2
1	4.0	3.88	1	4.0	3.88	1	4.0
1	6.1	3.53	1	6.1	3.53	1	6.1
1	9.2	3.17	1	9.2	3.17	1	9.2
1	4.0	3.88	1	4.0	3.88	1	4.0

Bearing in mind the previously mentioned assumption that the difference of velocity distribution in the near-wall Prandtl layer and the flow core is connected with a viscous component of skin friction drag, we can determine the $\frac{\tau_T}{\tau_\Sigma}$ correlation on the boundary of Prandtl layer for real values $\frac{u_{*0} r_0}{\nu}$ shown in table 4 for $\frac{y}{r_0} = \left(\frac{l_p}{r_0}\right)_B$. The calculation results

for $\frac{\tau_T}{\tau_\Sigma}$ based on formula (18) presented in Table 4 indicate that the velocity profile in the near-wall Prandtl layer exists if the viscous component of skin friction drag is barely noticeable.

The graphs of $\left(\frac{l_p}{r_0}\right)_B$ and $\frac{y_M}{r_0}$ change based on λ value (Fig. 2) show both the tendency of their quality similarity and quantitative difference. The dependency $\left(\frac{l_p}{r_0}\right)_B = f(\lambda)$ can be approximated as

$$\ln\left(\frac{l_p}{r_0}\right)_B = -0.5 - \frac{0{,}18}{\sqrt{\lambda}} \tag{19}$$

Analysis of experimental data for velocity distribution in pipes [20] and open channels [14] showed that velocity distribution in the flow core above the Prandtl layer could be quite accurately approximated as a logarithmic profile, similar to Prandtl layer:

$$\frac{u_{\max} - u}{u_*} = \frac{1}{\kappa_2} \ln \frac{r_0}{y} \tag{20}$$

However, the angular coefficient for this $\frac{1}{\kappa_2}$ profile is significantly different from the angular coefficient $\frac{1}{\kappa_1}$=2.44 for the Prandtl layer velocity profile.

To determine κ_2 value we can express the velocity profile for the flow core based on Hinze's ideas as:

$$\frac{u_{\max} - u}{u_*} = -2.44 \ln \frac{y}{r_0} + 0.8 + h\left(\frac{y}{r_0}\right) \tag{21}$$

where Hinze shows $h\left(\frac{y}{r_0}\right)$ function as a graph (Fig. 4).

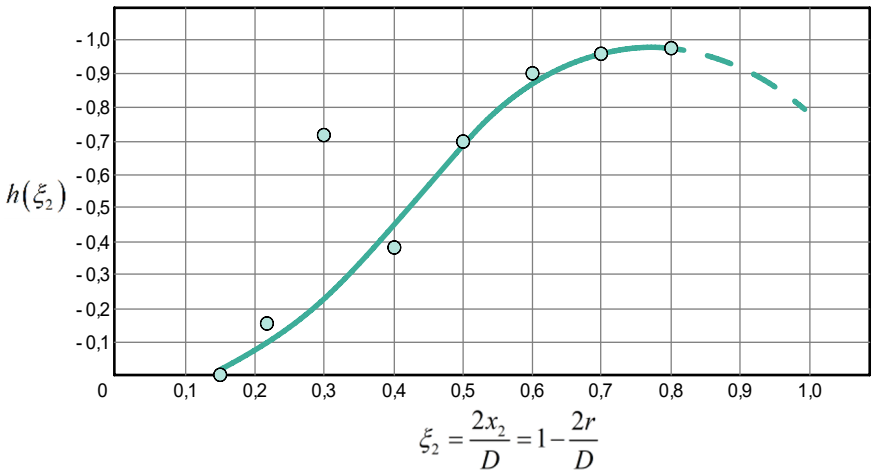

Fig. 4. Hinze function in graphical form

Considering the possibility of expressing the velocity distribution of the flow as a logarithmic profile, we can express $h\left(\frac{y}{r_0}\right)$ the function as the following logarithmic approximation that is accurate enough for experimental points in Fig. 3:

$$h\left(\frac{y}{r_0}\right) = \beta_T \ln\frac{y}{0.15r_0} = \beta_T \ln 6 + \beta_T \ln\frac{y}{r_0} \qquad (22)$$

where $0.15r_0$ is the average l_p value starting from which we need to use a correction additive for Prandtl–Nikuradse profile. At the same time, the velocity profile for the flow core can be expressed as

$$\frac{u_{\max} - u}{u_*} = -\frac{1}{\kappa_1}\ln\frac{y}{r_0} + 0{,}8 - \beta_T \ln 6 - \beta_T \ln\frac{y}{r_0} \qquad (23)$$

where $\frac{1}{\kappa_1}$=2.44 and β coefficient needs to be determined.

To determine β we can use the condition for speed deficiency to equal zero when $y=r_0$. Thus, we get

$0.8 = \beta_T \ln 6$,

hence β_T=0.44 (24)

Therefore, the expression (23) takes the following form:

$$\frac{u_{\max} - u}{u_*} = (2.44 + 0.44)\ln\frac{r_0}{y} = 2.88\ln\frac{r_0}{y} \qquad (25)$$

Then velocity profile logarithmic approximation for the flow core will have an average angular coefficient

$$\frac{1}{\kappa_2} = 2.88 \tag{26}$$

that is 1.18 times higher than the angular coefficient for the logarithmic velocity profile in the Prandtl layer.

According to Hinze [18], for the peripheral area of the flow in the flat plate boundary layer, the velocity deficiency profile can be expressed as

$$\frac{u_{\max} - u}{u_*} = -2.44 \ln \frac{y}{\delta} + 2.5 + h\left(\frac{y}{\delta}\right) \tag{27}$$

where correction additive $h\left(\frac{y}{\delta}\right)$ is shown as a graph in Fig. 5, and δ is the width of the boundary layer.

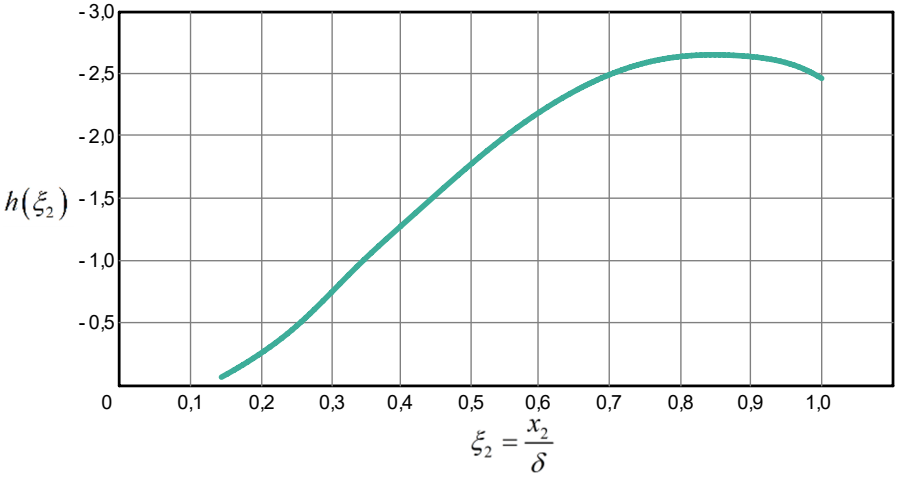

Fig. 5. Correction additive $h\left(\frac{y}{\delta}\right)$ in graphical form

For the correction additive, we can use an approximation like in formula (22)

$$h\left(\frac{y}{\delta}\right) = \beta_n \ln \frac{y}{0.15\delta} = \beta_n \ln 6 + \beta_n \ln \frac{y}{\delta} \tag{28}$$

Then we can express the velocity profile (27) as

$$\frac{u_{\max} - u}{u_*} = (2.44 + \beta_n) \ln \frac{\delta}{y} + 2.5 - \beta_n \ln 6 \tag{29}$$

where β_n value can be determined from the condition of $u=u_{max}$ with $y=\delta$.

$2.5 = \beta_n \ln 6$,

hence $\beta_n=1.39$.

Considering the determined β_n value, we can find the angular coefficient in expression (29).

$$\frac{1}{\kappa_2} = 2.44 + \beta_n = 2.44 + 1.39 = 3.83 \tag{30}$$

At the same time, velocity deficiency for the peripheral area of the boundary layer takes the following form

$$\frac{u_{\max} - u}{u_*} = 3.83 \ln \frac{\delta}{y} = 8.8 \lg \frac{\delta}{y} \tag{31}$$

Comparison of dependencies (25) and (31) shows that, while flowing in a pipe with an angular coefficient ratio equal to 1.33, in a quantitative sense, velocity distribution in the peripheral area of the flat plate boundary layer is significantly different than in flow core.

The determined angular coefficient in the logarithmic velocity profile for the outer zone of the boundary layer (29, 30) is consistent with the experimental value of the velocity profile angular coefficient measured in wide open smooth and rough channels (Fig. 6, 7).

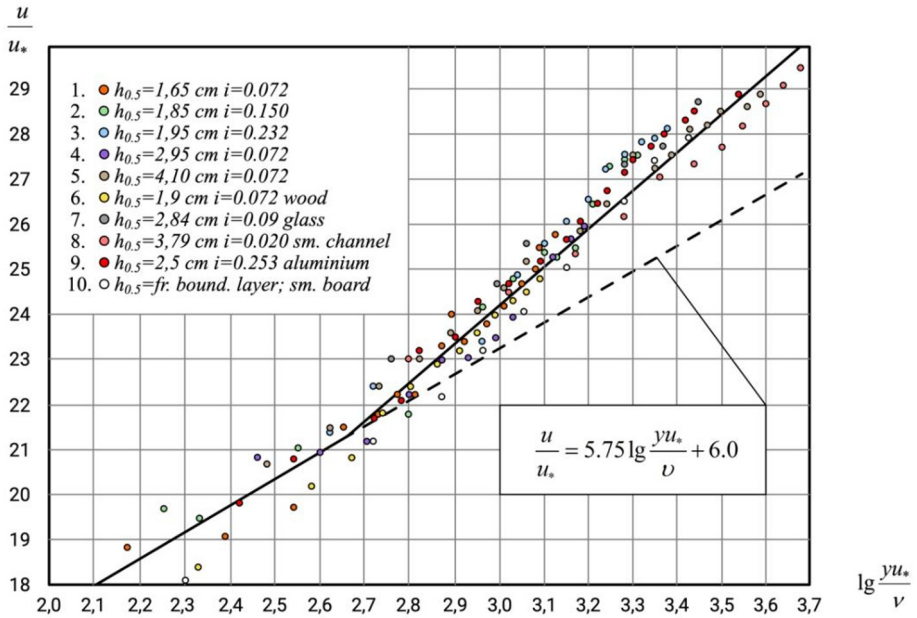

Fig. 6. Experimental value for velocity profile angular coefficient,
1-6 are V.S. Borovkov; 7 is L. Gogiberidze; 8 is M. Viparelli; 9 is L. Rao; 10 is G. Ludvig & V. Tilman.

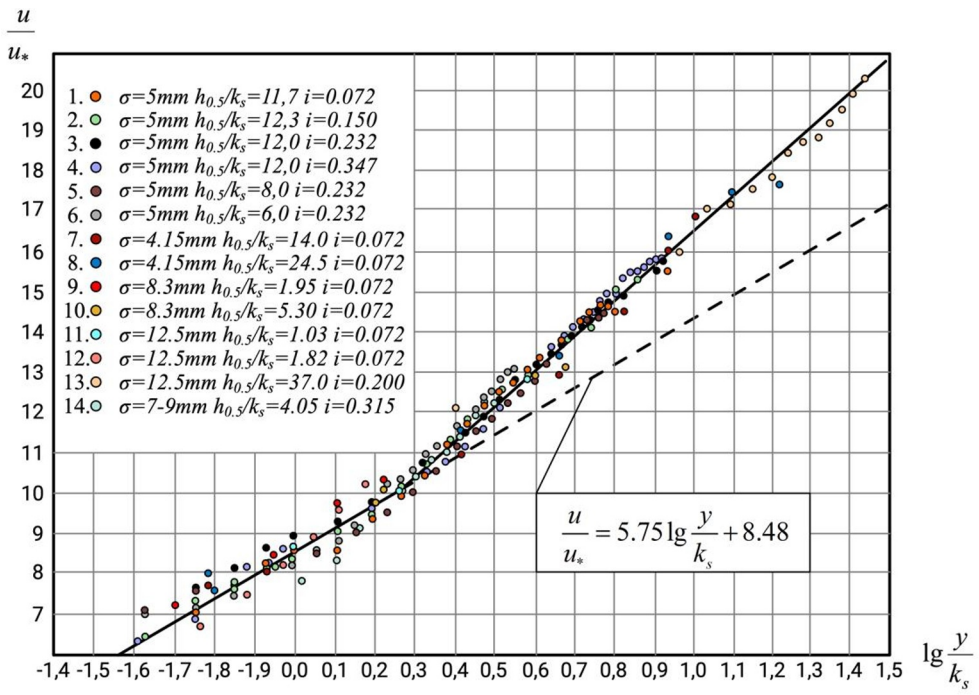

Fig. 7. Experimental value for velocity profile angular coefficient,
1-12 are V.S. Borovkov; 13 is M. Viparelli; 14 is N. Isachenko.

4 Conclusion

Conducted analysis shows that the maximum turbulent skin friction drag point is located at the distance of $(0.1 \div 0.15) r_0$. A comparison of the total amount of skin friction drag and its turbulent component allows us to conclude that the viscous component of skin friction drag has a significant contribution to the total drag. With the increase of λ value, the contribution of viscous component grows and exceeds 4–5% till $\frac{y}{r_0} \sim 0.25 \div 0.30$.

Based on the assumption that the difference in velocity distribution in the near-wall Prandtl layer and the flow core is connected with the viscous component of skin friction drag, it was possible to determine the correlation between turbulent skin friction drag. Total skin friction drag $\frac{\tau_T}{\tau_\Sigma}$ on the boundary of Prandtl layer. The calculation results show that the velocity profile in the near-wall Prandtl layer exists if the viscous component of skin friction drag is barely noticeable.

An angular coefficient of 1.33 is obtained in the logarithmic velocity profile for the outer zone of the boundary layer, confirming the assumptions about the flow similarity between boundary layers and wide open channels.

References

1. Pal, D., & Ghoshal, K. (2016). Vertical distribution of fluid velocity and suspended sediment in open channel turbulent flow. *Fluid Dynamics Research*, *48*(3). https://doi.org/10.1088/0169-5983/48/3/035501
2. Han, Y., Yang, S. Q., Sivakumar, M., & Qiu, L. C. (2017). Investigation of Velocity Distribution in Open Channel Flows Based on Conditional Average of Turbulent Structures. *Mathematical Problems in Engineering*, *2017*. https://doi.org/10.1155/2017/1458591
3. H.P Mazumdar, B.Ch. Mandal, Fully developed turbulent pipe flow, U.P.B. Sci. Bull. Series D **73** 99-110 (2011)
4. L.I. Vysotsky, Russian Scientific Research Institute of Land Improvement Problems **4** 125-138 (2012)
5. A. Zaryankin, A. Rogalev, V. Kindra, G. Kurdiukova, A. Vegera. On the compatibility of a logarithmic turbulent boundary layer velocity profile with experimental data // International Journal of Computational Methods and Experimental Measurements, (2016), 4 (4) DOI: 10.2495/CMEM-V4-N4-554-560
6. Constaín AJ. Prandtl's universal velocity distribution law in streams: a consequence of brownian nature of turbulence at dynamic equilibrium. International Journal of Hydrology (2018), 2 (2): 253-256. DOI: 10.15406/ijh.2018.02.00077
7. V. N. Bajkov, MSUCE Bulletin **4** 19-22 (2009)
8. L. D. Landau, Theoretical physics **6** 788 (1953)
9. Chung Yang, Han, Lun Chiang, Jie. A study of the river velocity measurement techniques and analysis methods // EGU General Assembly 2013, held 7-12 April, 2013 in Vienna, Austria, id. EGU2013-1692
10. E. Ignatenko, Yu. Bryanskaya. Velocity distribution in a turbulent flow // E3S Web Conf., 263 (2021) 04047. DOI: https://doi.org/10.1051/e3sconf/202126304047
11. A. Dmitrenko. Theoretical calculation of the laminar-turbulent transition in the round tube on the basis of stochastic theory of turbulence and equivalence of measures // Continuum Mechanics and Thermodynamics, Volume 34, Issue 6, p.1375-1392. doi: 10.1007/s00161-022-01125-4
12. Adrian, R. J., & Marusic, I. (2012). Coherent structures in flow over hydraulic engineering surfaces. *Journal of Hydraulic Research*, *50*(5), 451–464. https://doi.org/10.1080/00221686.2012.729540
13. H. W. Emmons, Aerospace Sciences **81** 150-152 (1951)
14. H. A. Einstein, H. Li, Journal Engineering Mechanical Division **82** (1956)
15. A.I. Bogomolov, V.S. Borovkov, F.G. Majranovskij, High-speed flows with a free surface (1979)
16. Y.V. Bryanskaya, I.M. Markova, A.V. Ostyakova Hydraulics of water and suspended flows in rigid and deformable boundaries (2009)
17. V.S. Borovkov, V.V. Volshanik, I.A. Rylova. Peculiarities of velocity distribution in turbulent flow // MSUCE Bulletin. 2015 №6. С.103-109.
18. I. O. Hinze, Turbulence. An introduction to its mechanism and theory (1963)
19. Coles D.J. Fluid Mech., 1, 191, 1956.

20. Yu. Bryanskaya. Refinement of velocity profile parameters for flows in smooth and rough pipes // International Journal of Applied Engineering Research. 2016. Volume 11, Number 3 (2016), pp. 1694-1698
21. Schlichting H. Boundary Layer Theory. M.: Nauka, 1969.